Carbohydrate Polymers 101 (2014) 760–768

Contents lists available at ScienceDirect

Carbohydrate Polymers

journal homepage: www.elsevier.com/locate/carbpol

Synthesis and characterization of dextran stabilized superparamagnetic iron oxide nanoparticles for in vivo MR imaging of liver fibrosis

Ariya Saraswathy[a], Shaiju. S. Nazeer[a], Nirmala Nimi[a], Sabareeswaran Arumugam[b], Sachin. J. Shenoy[c], Ramapurath. S. Jayasree[a,*]

[a] Biophotonics and Imaging Lab, Biomedical Technology Wing, Sree Chitra Tirunal Institute for Medical Sciences & Technology, Poojappura, Thiruvananthapuram 695 012, Kerala, India
[b] Division of Implant Biology, Biomedical Technology Wing, Sree Chitra Tirunal Institute for Medical Sciences & Technology, Poojappura, Thiruvananthapuram 695 012, Kerala, India
[c] In Vivo Models and Testing Division, Biomedical Technology Wing, Sree Chitra Tirunal Institute for Medical Sciences & Technology, Poojappura, Thiruvananthapuram 695 012, Kerala, India

ARTICLE INFO

Article history:
Received 17 June 2013
Received in revised form 4 September 2013
Accepted 4 October 2013
Available online 12 October 2013

Keywords:
Liver fibrosis
Superparamagnetic iron oxide
Magnetic resonance imaging
Dextran
Hepatocellular uptake

ABSTRACT

The field of medical imaging has recently seen rapid advances in the development of novel agents for enhancing image contrast. In particular, superparamagnetic iron oxide nanoparticles (SPIONs) with a variety of surface properties have been tried as effective contrast agents for magnetic resonance imaging, but with major side effects. In this study, the surface chemistry of SPIONs of size 12 nm was modified with high molecular weight dextran to yield particles of size 50 nm, without compromising the magnetic properties. A systematic characterization of the material for its size, coating efficiency, magnetic properties and biocompatibility has been carried out. The magnetic relaxivity as evaluated on a 1.5 T clinical magnet showed r_2/r_1 ratio of 56.28 which is higher than that reported for any other dextran stabilized ironoxide nanoparticles. Liver uptake and magnetic resonance imaging potential of dextran stabilized SPIONs (D-SPIONs) has been evaluated on liver fibrosis induced animal model, which is further supported by histopathology results.

1. Introduction

Magnetic resonance imaging (MRI) is a potential tool for in vivo evaluation of diseases with high spatial resolution. Though the technique provides images with intrinsic contrast, for the extensive diagnostic information, extrinsic agents which could enhance the contrast of the images with respect to different pathology becomes necessary in majority of the cases. SPIONs with appropriate surface chemistry have been widely used as a tool to enhance image contrast in MRI of liver and lymph nodes (Chung et al., 2012; Reimer & Balzer, 2003; Vu-Quang et al., 2012a,b; Wang, Hussain, & Krestin, 2001; Weinstein et al., 2010). A systematic approach to the physiochemical and biological characterization of these groups of materials is missing.

Liver cancer is the fifth most frequently diagnosed cancer among men and seventh most commonly diagnosed cancer among women. Also it is the second and sixth most frequent cause of cancer death among men and women respectively (Jemal, Bray, Center, Ferlay, Ward, & Forman, 2011). Chronic alcoholism is one of the major reasons behind this devastating incidence of liver cancer. If diagnosed at an early stage most of the liver cancer related to alcoholism is reversible and curable. Liver diseases associated with alcoholism are classified as fibrosis and cirrhosis depending on the degree of damage caused by alcohol. Among this, cirrhosis is the advanced stage and the most prevalent causes of alcohol related death (Mann, Smart, & Govoni, 2003; Szabo & Mandrekar, 2010).

In liver associated malignancies, over expression of asialoglycoprotein receptors occur which has got a carbohydrate recognition domain (Reimer, Weissleder, Lee, Buettner, Wittenberg, & Brady, 1991; Stefanescu, Born, Moise, Ernst, & Przybylski, 2011; Veselkin et al., 2011). The presence of this domain could be exploited in modifying the surface of the nanomaterials with carbohydrate polymers to enhance passive uptake. This property enables SPIONs with carbohydrate polymers to specifically target to liver and hence can be used as contrast agents in diseases associated with hepatic diseases. Many reports are available on the use of SPIONs with various surface stabilizing agents such as dextran, citrate and polyethylene glycol. The most studied one

* Corresponding author. Tel.: +91 4712520273; fax: +91 471 2341814; mobile: +91 9495948221.
E-mail addresses: jayashreemenon@gmail.com, jayasree@sctimst.ac.in (Ramapurath.S. Jayasree).

0144-8617/$ – see front matter © 2013 Elsevier Ltd. All rights reserved.
http://dx.doi.org/10.1016/j.carbpol.2013.10.015

being the dextran coated SPIONs (Hradil, Pisarev, Babic, & Horak, 2007; Saboktakin, Tabatabaie, Maharramov, & Ramazanov, 2010a; Saboktakin, Tabatabaie, Maharramov, & Ramazanov, 2010b). Dextran is a naturally occurring water soluble polysaccharide found in certain lactic-acid bacteria *Leuconostoc mesenteroides* and *Streptococcus mutans*, composed of α-D-(1 → 6) linked glucose units and some α-D-(1 → 3) linked glucose branch units in varying proportions and sequential arrangements (Molday & MacKenzie, 1982). Dextran has got many advantages like its biocompatibility, biodegradability and improved transfection efficiency which makes it suitable for use in biological systems. It is also inexpensive, non-toxic and easily available (Thomas, Rekha, & Sharma, 2012). Also, dextran stabilized magnetite particles showed prolonged blood residence time which allows access to macrophages located in certain tissues such as lymph node, liver, kidney, etc. (Molday & MacKenzie, 1982). These favourable factors were considered while choosing stabilizing agent for SPIONs as dextran for developing liver specific MR contrast agents.

Few of the SPIONs based contrast agents like Endorem, Resovist, Clariscan had been previously approved for clinical use, especially for liver/lymph node MRI (Reimer & Balzer, 2003; Wang, 2011; Weinstein et al., 2010). Later these products were withdrawn from the market due to insufficient clinical trial results and major safety concerns (Wang, 2011; Web ref.). It is understood that the surface modification of these contrast agents were mainly based on biopolymers like dextran with low molecular weight (Simberg et al., 2009; Weinstein et al., 2010). But it is reported that dextran with molecular weights below 60 kDa will easily filter through the glomerulus and cause osmotic nephropathy which leads to chronic renal failure (Feest, 1976; Morgan, Little, & Evans, 1966). This would have been one of the reasons of safety concerns and subsequent withdrawal of the dextran based contrast agents from the market. A similar problem has also been reported with the administration of Gadolinium based positive contrast agents (Marckmann et al., 2006; Yerram, Saab, Karuparthi, Hayden, & Khanna, 2007). Thereafter, none of the research groups have attempted to address this issue. Considering these factors, we have adopted a synthesis strategy and developed a high molecular weight dextran stabilized SPIONs for contrast enhanced liver MRI. But the use of high molecular weight and long branched polymers as coating agents has disadvantages like increased coating thickness which would further increase the particle size considerably and also decrease the magnetic property. Development of the particles without compromising the size and magnetic properties is really challenging.

In this study, SPIONs with particle size of 12 nm were prepared and used to get D-SPIONs with hydrodynamic size of 50 nm which showed excellent magnetic relaxivity and enhanced magnetic saturation. Also, D-SPIONs demonstrated good blood and cell compatibility at even higher concentrations and very good cellular labelling efficiency. The efficiency of the developed system has been successfully demonstrated in a rodent model of liver fibrosis to enable early diagnosis of liver damage.

2. Materials and methods

2.1. Synthesis of D-SPIONs

$FeCl_3$ anhydrous, $FeCl_2{\cdot}4H_2O$, NaOH, 35% HCl (all from Merck, Germany/India) and Dextran (Mw-70,000) (Sigma Life Science) were used for the preparation of D-SPIONs. The chemicals used in the cell culture studies were 3-(4,5-dimethylthiazol-2-yl)-2,5-diphenyl tetrazolium bromide (MTT), Eagle's minimum essential medium, sodium bicarbonate, Gentamicin (Himedia, Germany), Amphotericin B solution and FBS (Sigma–Aldrich, Germany).

SPIONs were prepared by alkaline co-precipitation of Ferrous and Ferric salts in aqueous solution. Briefly, $FeCl_3$ and $FeCl_2{\cdot}4H_2O$ in 100 ml deionized water were mixed in the 2:1 molar ratio and magnetically stirred at a temperature of 80 °C. The alkaline mixture is slowly precipitated with 1 M NaOH at a pH of 12. Black precipitate resulted indicating the formation of ironoxide nanoparticles and the system was allowed to continue under the same reaction condition for 2 h to ensure complete precipitation. The precipitate was magnetically separated and the residue was washed and the pH adjusted to collect water dispersed particles. The ironoxide nanoparticles formed were dispersed in 3% dextran and stirred for 6 h at 80 °C. The suspension was washed with deionized water and centrifuged.

2.2. Characterization of particles

2.2.1. Size, phase and morphometric analysis

The size and morphology of D-SPIONs were examined by high resolution transmission electron microscopy at 100 kV (HRTEM, Hitachi-JEOL, Tokyo, Japan). Hydrodynamic size and the surface charge of the prepared nanoparticles were measured using a dynamic light scattering system (DLS, Zetasizer NanoZS90, Malvern Instruments Ltd., Worcestershire, UK).

The phase analysis of D-SPIONs was carried out using X'Pert PRO X-ray diffraction (XRD) unit. Crystal structure was determined by analyzing the position and intensity of diffraction peaks observed in the diffraction angle in the range, $2\theta = 10°–80°$ using Cu Kα radiation of 1.5406 Å at 40 kV and a 20 mA current. The diffraction pattern also yielded the crystallite size from the width and shape of the peak profile using Scherrer equation.

2.2.2. Surface characterization

Fourier transform infrared (FTIR) spectra of D-SPIONs and dextran were recorded using Thermo Nicolet 5700 FTIR spectrometer (USA) in the diffuse reflectance mode. To enable high signal to noise ratio, 64 scans were acquired at a resolution of 4 cm^{-1}.

The thermal properties of the prepared material were assessed using thermo gravimetric analysis (TGA) using SDT 2960 V2.2B (simultaneous TGA-DTA, TA Instruments, Delaware, USA) instrument which was also used to evaluate the amount of dextran bound to the ironoxide nanoparticles. The experiment was run under oxygen atmosphere with in a temperature range of 25–1200 °C applying a constant heating rate of 10 °C/min. The percentage of weight loss at different stages accounted for the degradation of the organic content present in the sample.

2.2.3. Characterization of magnetic properties

The magnetic property of SPIONs and D-SPIONs was measured at room temperature using a Lakeshore model 7410 vibrational sample magnetometer (VSM). The magnetic hysteresis and saturation magnetization of SPIONs and D-SPIONs were evaluated.

For measuring the magnetic relaxation property of the material, MR images of D-SPIONs suspensions were acquired using a clinical, 1.5 T whole body MR scanner (MAGNETOM Avento Tim System 1.5 T, Siemens, Munich, Germany) using a 12 channel head coil. A series of study with iron concentrations of 0.45, 0.225, 0.1125, 0.05625, 0.028125 and 0.0 mM was performed using aqueous phantoms. An inversion recovery sequence with constant repetition time (TR) and echo time (TE) of 4000 and 11 ms respectively with varying inversion time (TI) of 50, 100, 300, 700, 1200, 2000 and 3000 ms was used for calculating longitudinal relaxation rate (r_1). A modified transverse relaxometry spin echo sequence with TR of 2000 ms with varying TE from 15 to 150 ms was used for getting transverse relaxation rate (r_2). Both sequences were run at three different planes of the phantoms with a slice thickness of 10 mm.

Pixel intensity with respect to each concentration was extracted from the resulting MRI maps. Signal intensity against TI and TE values were plotted for getting T_1 and T_2 relaxation times respectively. Likewise, T_1 and T_2 relaxation times for different concentration were obtained. These values were plotted against the iron concentrations. Longitudinal and transverse relaxation values (r_1 and r_2) were calculated by the linear fit as reported elsewhere (Nidhin, Nazeer, Jayasree, Kiran, Nair, & Sreeram, 2013; Wan, Jiang, Li, & Chen, 2012)

2.2.4. Biocompatibility evaluation

2.2.4.1. Blood compatibility studies. For haemolysis study, 800 μl of separated human RBC was taken and made up to 3 ml with saline and mixed gently. Then 900 μl of 100 μg/ml D-SPIONs dispersed in saline was added to 100 μl of washed RBC, mixed gently and incubated for 2 h. The sample was centrifuged for 5 min at 1500 rpm and to the supernatant solution 900 μl of saline was added and the absorption at 541 nm was recorded using UV spectrophotometer (Carywin UV). Saline was used as the negative control and distilled water as positive control to calculate the percentage haemolysis.

For blood aggregation study, 100 μl of 100 μg/ml of the D-SPIONs were added to 100 μl of diluted RBC, WBC and platelet separately and incubated for 30 min at 37 °C. Aggregation was visually assessed through phase contrast microscope (Leica DM IRB, Germany). Saline was used as negative control and polyethylene imine (PEI) as positive control.

2.2.4.2. Cellular interaction. Cytotoxicity of D-SPIONs on hepatocellular carcinoma cells, Hep G2, was assessed by standard MTT assay in triplicate. Different concentrations of D-SPIONs (100, 50 and 25 μg/ml), negative and positive controls were added to the cells and incubated for 24 h. On removal of the media, MTT (0.2 mg/ml) was added to each well and again incubated for 3 h. On removal of MTT, dimethyl sulfoxide was added to dissolve the formed formazan crystals and incubated for 30 min. Absorbance was quantified based on the peak at 570 nm using micro plate reader (Biotech, Power wave XS, USA).

2.2.5. In vivo studies

2.2.5.1. Animal model development and in vivo MRI studies. All studies involving animals were approved by the Institutional Animal Ethics Committee of Sree Chitra Tirunal Institute for Medical Sciences and Technology. The animal model for liver fibrosis was developed as per reported protocol of Constandinou, Henderson, & Iredale, 2005. Briefly, male Wistar rats weighing 200–250 g were treated twice a week, intraperitoneally, with equal parts of CCl_4 and olive oil for 6 weeks. For the initial two weeks, 0.2 ml/100 g of the CCl_4-olive oil mix was administered and the dose was reduced to 0.1 ml/100 g for the subsequent weeks. Development of liver fibrosis was confirmed by liver function test for the liver enzyme serum glutamic oxaloacetic transaminase (SGOT) and serum glutamic pyruvic transaminase (SGPT) at the end of six weeks. Post MRI histopathology of the organ also confirmed the developed fibrosis.

Animal MRI studies were performed on a 1.5 T clinical magnet running a multisection T_2-weighted turbo spin echo sequence (TR 5780 ms; TE 125 ms; FOV 98 mm × 140 mm; slice thickness 3 mm; flip angle 90). Animals were anaesthetized using ketamine and xylazine at a dosage of 70 mg/kg and 5 mg/kg of body weight. The contrast agent (D-SPIONs) was administered through tail vein at a dose of 2.17 mg/ml (0.04 mM) Fe/kg body weight. MRI scan was performed before and after 5 min of contrast agent administration. Signal intensity corresponding to pre and post contrast images was extracted and the percentage signal intensity change was calculated.

2.2.5.2. Histological analysis. Animals were sacrificed after 2 h of D-SPIONs injection to remove the liver for histological analysis. The tissues were fixed with 10% neutral buffered formalin and embedded in paraffin and sectioned. The sections were stained with haematoxylin–eosin (H&E) for histological analysis. Masson's trichrome (MT) and Pearls' Prussian blue (PB) staining was done to assess the degree of fibrosis as exhibited by the collagen fibres and the presence of iron in the liver, respectively.

3. Results and discussion

The SPIONs of desired particle size were synthesized by optimizing reaction conditions at a controlled pH and the ionic concentration of the medium by a co-precipitation method. The electrostatic interaction of hydroxyl group of dextran with iron atom at the ambient conditions resulted in the production of DSPIONs with optimum size. To maintain the overall particle size and the magnetic property of the D-SPIONs when using a high molecular weight stabilizing agent, the % w/v of dextran was adjusted. The results of various physico-chemical and magnetic characterizations, in vitro cytotoxicity, blood compatibility assessments and animal imaging are presented.

3.1. Size and phase analysis

The particle size analysis was carried out using TEM, DLS and XRD techniques. The uniform size distribution and nearly spherical morphology of the D-SPIONs is clear from the TEM micrograph. The dextran coating of SPIONs prevents the particles from aggregation, which is also clear from the well dispersed appearance of D-SPIONs in the HRTEM micrographs (Fig. 1a). Here, the average particle core size was found to be about 12 nm. DLS shows a hydrodynamic diameter of 50 nm (Fig. 1b). The XRD pattern (Fig. 1c) confirms the inverse spinal structure of magnetite with the indices (1 1 1), (2 2 0), (3 1 1), (2 2 2), (4 0 0), (4 2 2), (5 1 1) and (4 4 0) as per the JCPDS Card No. 89-0691. From the Debye–Scherrer equation, a crystallite size of the D-SPIONs was estimated as 8.52 nm.

3.2. Surface characterization

Surface coating of magnetite nanoparticles was confirmed by different surface characterization techniques including FTIR, TGA and Zeta-potential analysis.

The FTIR of D-SPIONs exhibited distinct peaks around 1461, 1344, 1000 cm^{-1} which corresponds to the —C—H and —C—O deformations of dextran (Fig. 2a). Absence of the peak corresponding to —OH and the presence of Fe-O band around 580 cm^{-1} confirmed the hydroxyl interaction with iron (Bautista, Bomati-Miguel, Morales, Serna, & Veintemillas-Verdaguer, 2005). For the accurate assignments of the peak, second derivative infrared spectra were considered (Fig. 2b).

TGA studies of D-SPIONs and free dextran in the range 0–1200 °C and the corresponding thermal decomposition curves are shown in Fig. 3. Free dextran shows three distinct degradation stages at 118, 357 and 492 °C with a corresponding total weight loss of 10, 77 and 100%. The decomposition starts with elimination of bound water at around 118 °C followed by the breakdown of organic skeleton around 357 °C and a complex degradation process in the temperature range of 257–492 °C resulting in the complete degradation of the dextran indicating total weight loss at 492 °C. The TGA curve of D-SPIONs also shows corresponding stages of degradation around 120 °C with a weight loss of 2.31% and around 320 °C with a weight loss of 8.94%. At around 490 °C a total weight loss is observed, which in turn indicates the complete dissociation of dextran from the magnetite. Due to the catalytic effect of iron, an early dissociation of dextran from the magnetite binding is expected which could be

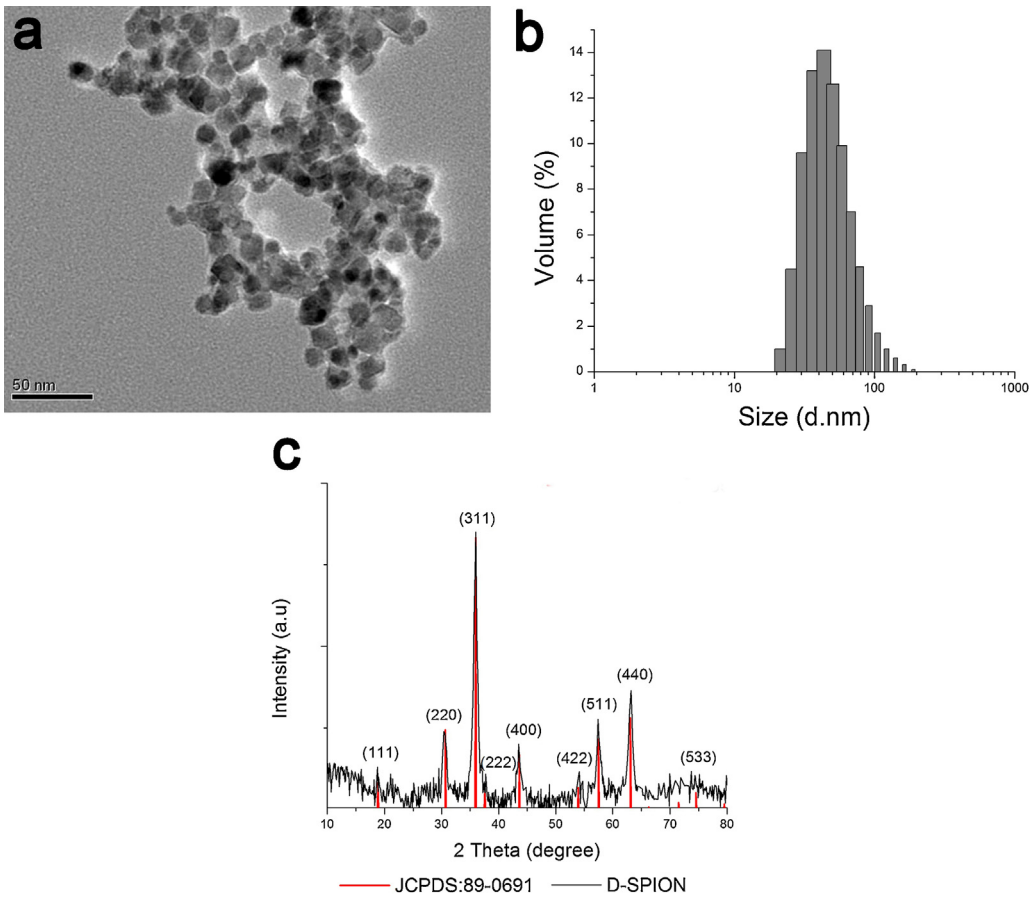

Fig. 1. Size and phase analysis of D-SPIONs. (a) HRTEM image shows spherical morphology and average particle size of 12 nm. (b) Hydrodynamic size distribution of D-SPIONs shows an average size of 50 nm. (c) Magnetite phase determination of D-SPIONs using X-ray diffraction pattern.

the reason for the observed shift in the degradation temperature of D-SPIONs from that of the free dextran. Carp et al. have reported similar decomposition pattern in an extensive thermal decomposition study of dextran coated magnetite nanoparticles (Carp, Patron, Culita, Budrugeac, Feder, & Diamandescu, 2010).

The zeta potential analysis of D-SPIONs showed a surface charge of −5.5 mV with the isoelectric point at pH 5.68. The negative zeta potential contributed by the dextran coating helped to maintain the stability of the colloidal system for long period of time (Jahn et al., 2011; Thomas, Rekha, & Sharma, 2010). This finding is an indication of the formation of flat layer of dextran with long polymeric chains over the SPIONs. Similar observation has been reported for starch coated stable suspension of magnetic nanoparticles (Kim et al., 2003).

3.3. Magnetic property evaluation

The magnetic property of the particles depends upon their structure, size, shape and chemical phase. The magnetic hysteresis loop of SPIONs and D-SPIONs studied by VSM are shown in Fig. 4a. Superparamagnetic property of both particles is clearly demonstrated by the zero coercivity. This property is a prerequisite for

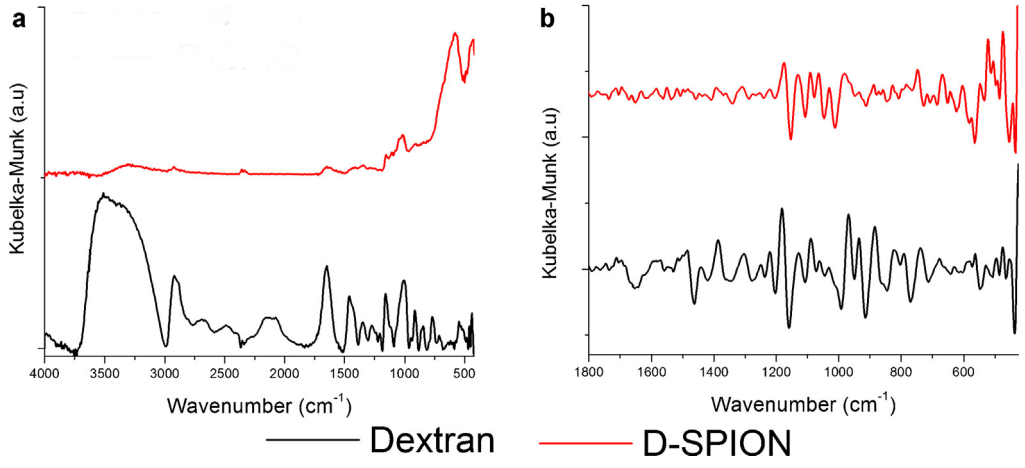

Fig. 2. FTIR spectra of (a) D-SPIONs and dextran (b) second derivative infrared spectra show the peaks corresponding to the exclusive vibrations of dextran in D-SPIONs.

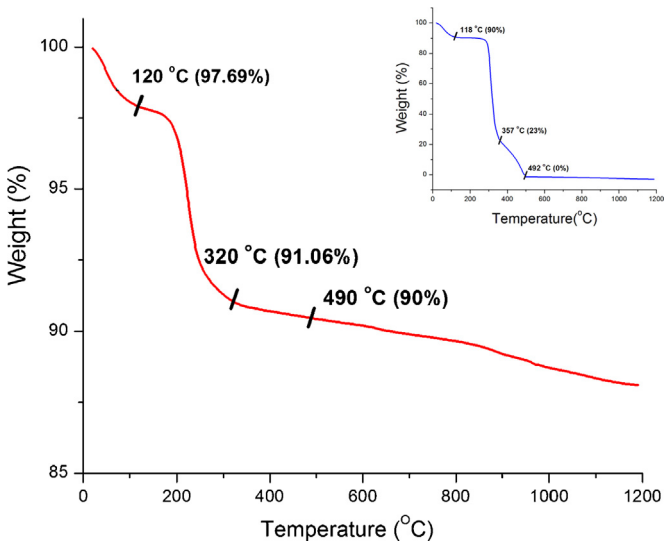

Fig. 3. Thermogravimetric analysis (TGA) curve of D-SPIONs which shows the thermal decomposition of dextran. TGA curve of pure dextran is given as inset figure.

the particles to demonstrate relaxivity property suitable for T_2 contrast agents. It is also reported that superparamagnetic property helps in the uniform dispersion of the particles in solution without the occurrence of severe aggregation that ferromagnetic nanoparticles usually suffer from (Manju, Sharma, & Sreenivasan, 2011). Hence superparamagnetic property is important for smooth circulation of the material through the blood. Saturation magnetization of the SPIONs was found to be 62.7 emu/g and that of D-SPIONs as 45.87 emu/g. This result confirms the preservation of magnetic properties of D-SPIONs even after the surface coating with dextran. The observed pattern of the hysteresis curve is an indication of the particle's single domain existence with only one orientation of magnetic moment. Here, the magnetization reduces from plateau region to zero on removal of the magnetic field. This further supports the magnetite phase of the developed material (Gupta & Wells, 2004).

The effect of D-SPIONs on the longitudinal (T_1) and transverse (T_2) proton relaxation was evaluated using a 63 MHz (1.5 T) clinical magnet. The magnetic susceptibility of the iron oxide nanoparticle generates local field gradients which in turn accelerate the dephasing of the spins of the surrounding water molecules enhancing spin–spin relaxation time (T_2). This is demonstrated as a gradual signal drop of the phantom images with increasing concentration of Fe. Relaxation images of D-SPIONs and r_2 value calculated from the slope of linear plots of $1/T_2$ versus concentration are given in Fig. 4b. High relaxivity value of 140.7 $mM^{-1}\,s^{-1}$ exhibited by D-SPIONs depends mainly on the effect of the delay in relaxation of the protons bound to the dextran coated SPIONs system. The high magnetic moment induced by the strong magnetic inhomogeneity around the particle causes high T_2 relaxivity.

Increase in pixel intensity of the phantom images with the increase in Fe concentration was observed for the T_1 weighed MR images also, even though the increase was not very significant. T_1 weighed MR images and r_1 values calculated by the linear fit are given in Fig. 4b. Longitudinal relaxivity value of 2.5 $mM^{-1}\,s^{-1}$ was observed for D-SPIONs. It has been reported that SPIONs of size less than 50 nm exhibits T_1 contrast in addition to T_2 contrast when used in moderate concentrations (Gossuin, Gillis, Hocq, Vuong, & Roch, 2009; Soenen, Hodenius, & De Cuyper, 2009). Ratio between transverse and longitudinal relaxivity (r_2/r_1) is an important parameter to estimate the efficiency of a contrast agent. In this study, r_2/r_1 ratio of 56.28 was observed. This is better than many of the iron oxide based contrast agents reported so far (Tsai et al., 2012).

3.4. Biocompatibility evaluation

3.4.1. Blood compatibility

The results of percentage hemolysis analysis of different concentrations of D-SPIONs showed no lysis when the particles were in contact with the erythrocytes. The percentage of lysis was found to be less than 1% with D-SPIONs.

Aggregation study of D-SPIONs with human RBC, WBC and platelet did not show any aggregation or morphological change under microscopic view, compared to the positive control PEI in any of the cases (Fig. 5).

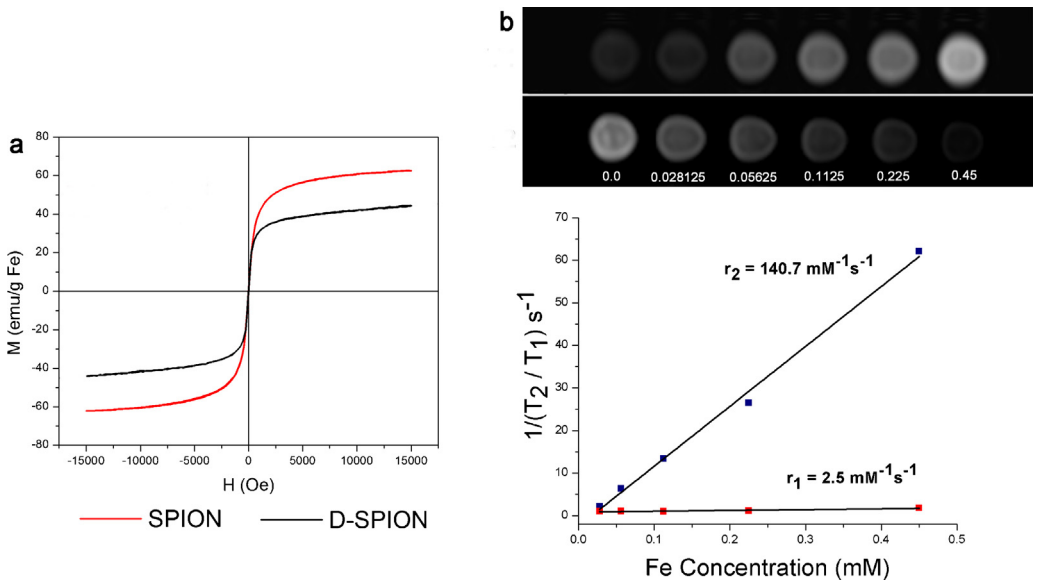

Fig. 4. Studies on the magnetic properties of D-SPIONs. (a) Magnetic hysteresis pattern is typical of superparamagnetic materials. Magnetic saturation values are also clear from the curves. (b) T_1 and T_2 weighted MR phantom images of D-SPIONs for varying concentrations (0–0.45 mM) and (c) longitudinal (r_1) and transverse (r_2) relaxation rate of D-SPIONs.

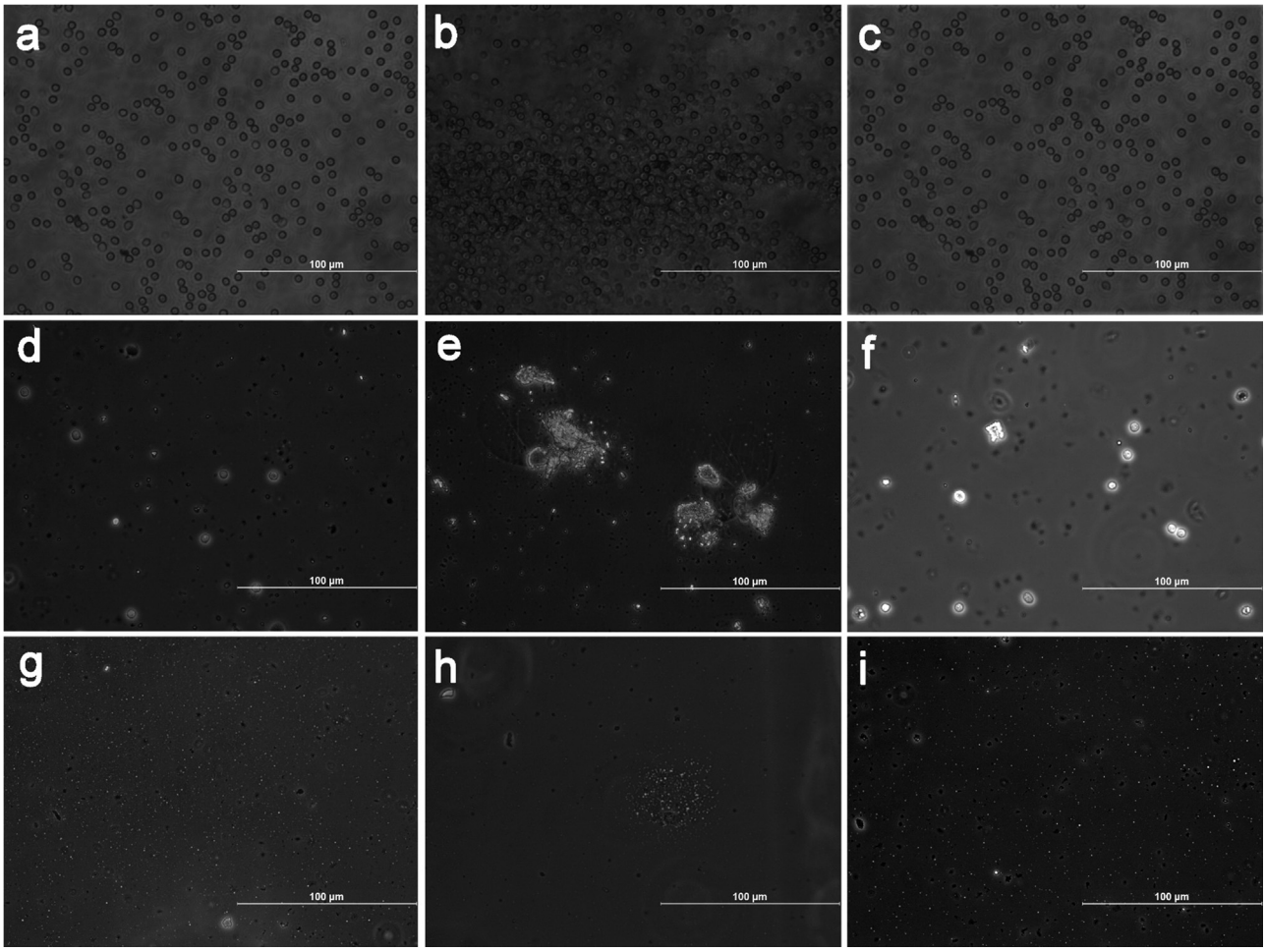

Fig. 5. Blood aggregation studies: RBCs incubated with (a) D-SPIONs (b) positive control, PEI and (c) negative control, saline; WBCs incubated with (d) D-SPIONs (e) PEI and (f) saline and platelets incubated with (g) D-SPIONs (h) PEI and (i) saline.

3.4.2. Cytotoxicity

As the aim of the study is to use the developed nanoparticles as MR contrast materials for liver fibrosis, it is important to see the toxicity effect of the particles on liver cells. For this, cytotoxicity of the nanoparticles was evaluated on human hepatocellular cells, HepG2 using MTT assay (Fig. 6). 82–100% viability of the cells was observed for 100–25 μg/ml concentrations of the D-SPIONs. Compared to previous reports on magnetic nanoparticles, D-SPIONs in the present study showed better cell viability at the respective concentrations (Gonzales, Mitsumori, Kushleika, Rosenfeld, & Krishnan, 2010; Wang & Cuschieri, 2013).

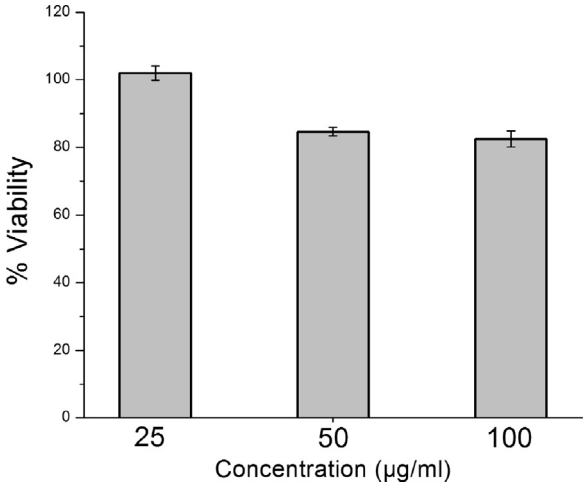

Fig. 6. Cytotoxicity studies of different concentrations (25, 50 and 100 μg/ml) of D-SPIONs using HepG2 cells.

3.5. In vivo MR imaging

The liver uptake potential and imaging efficiency of the D-SPIONs were demonstrated by the in vivo MR imaging of liver fibrosis in animal models. The development of animal model for liver fibrosis was confirmed by monitoring the liver transaminases SGPT and SGOT levels, which are biomarkers of liver injury. At the end of sixth week these markers were significantly high in fibrosis induced animals compared to control animals (Fig. 7a). Pre and post contrast T_2 weighted coronal and corresponding pseudo coloured images of the liver fibrosis induced animals are shown in Fig. 7b–e. D-SPIONs enhances the image contrast of tissues through considerable shortening of T_2 relaxation times. This shortening of T_2 relaxation leads to signal drop with the decrease in the pixel intensity at the sites where the SPIONs are accumulated.

The liver macrophages, the Kupffer cells, which are actively present in the pathogenesis of the liver diseases will increase the uptake of the iron in the liver (Piperno, 1998). Additionally, the over expression of receptors which has got affinity for carbohydrates also helps in the uptake of D-SPIONs in the liver. Also the small size of nanoparticles increases the accumulation of the same due

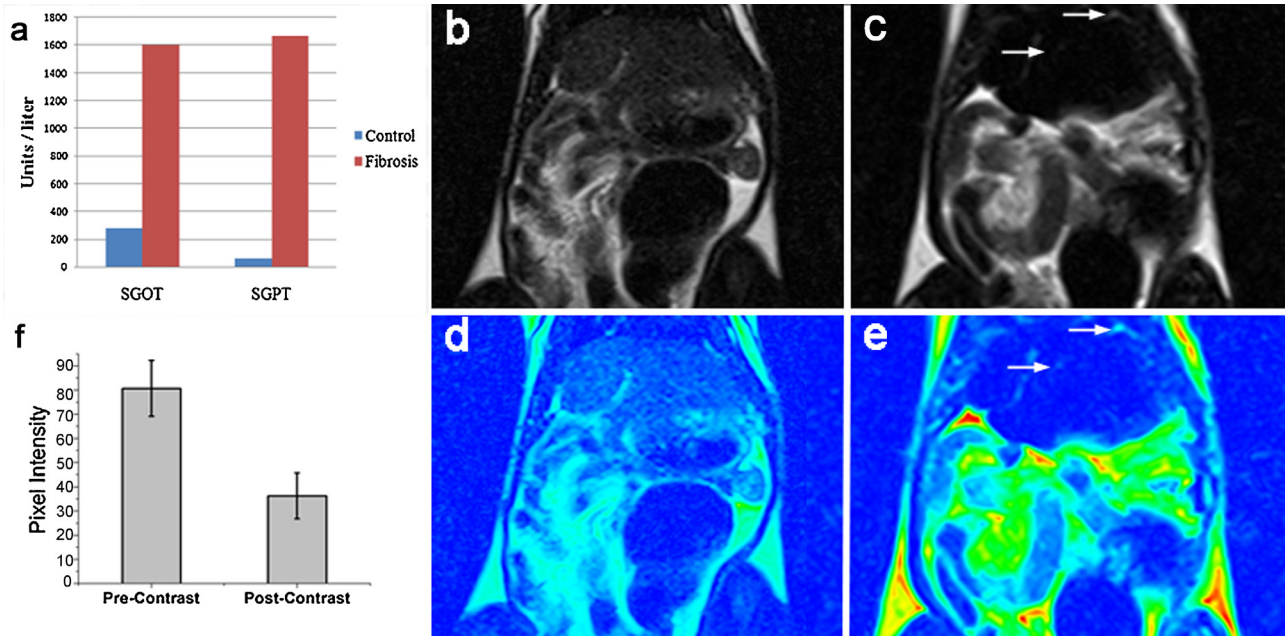

Fig. 7. (a) Liver function test of fibrosis induced and control animals. Pre (b) and post(c) contrast in vivo MR images of liver fibrosis rat model (d) and (e) represents the pseudo coloured images of the original MR images b and c. (f) Pixel intensity of liver from pre- and post contrast.

to the enhanced permeability and retention effect of D-SPIONs in the fibrosed liver (Albanese, Tang, & Chan, 2012). The heavy uptake of the D-SPIONs due to several factors shows a hypointense liver in the post contrast T_2 weighted images (Fig. 7f). The average signal intensity varies from 80.7 ± 11.6 for pre-contrast to 36.24 ± 9.44 for post-contrast images with a 55% decrease, which is very well appreciated with naked eye without any further image processing.

The optimized particle size, charge and surface chemistry increased the accumulation of D-SPIONs in the liver. Pathologically, liver fibrosis involves the over activation of hepatostellar cells, sinusoidal endothelial cells and Kupffer cells present in the hepatic sinusoid which triggers the overproduction of extracellular matrix and the impairment of degradation process resulting in the accumulation of tough, fibrous scar tissue in the liver (Van de Bovenkamp, Groothuis, Meijer, & Olinga, 2007). This increase in fibrogenesis and decrease in fibrolysis favours the passive targeting of the D-SPIONs at the liver fibrosis site (Albanese et al., 2012). At an advanced stage of fibrosis, nodular formation and subsequent decrease of Kupffer cell density in the scarred tissue occurs (Kolios, Valatas, & Kouroumalis, 2006; Talwalkar, Yin, Fidler, Sanderson, Kamath, & Ehman, 2008). In this situation the passive targeting of the particles will not be effective and appear as hyperintense structures (Curvo-Semedo, Brito, Seco, Costa, Marques, & Caseiro-Alves, 2010). These localized areas are well differentiated in the post contrast images as hyperintense streaks (Fig. 7c). This

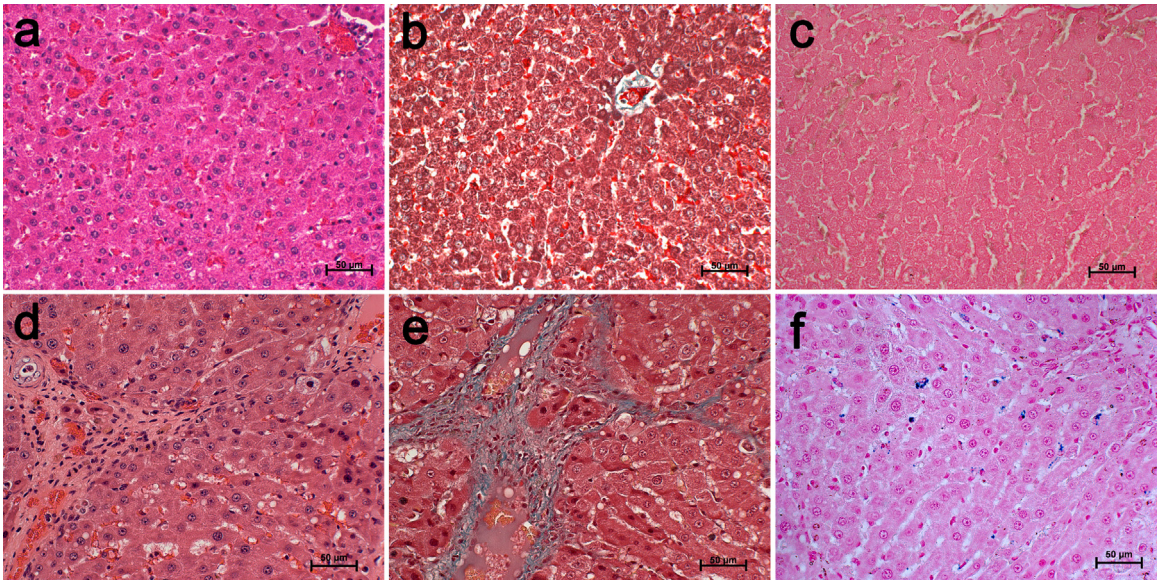

Fig. 8. Histopathological examinations of liver from normal and fibrosis model. H&E stained sections of normal liver (a) shows lobular architecture with central vein and radiating hepatic cords, fibroses liver (d) shows the disruption of the tissue architecture, extension of fibres and pseudo-lobe separation. MT staining of fibrosed liver (e) shows the presence of fibrous accumulation which is not seen in the case of normal section (b). PB stained sections shows the presence of iron in the D-SPIONs administered fibrosed liver (f) which is not seen in the case of normal liver (c).

contrast difference in the MR images helps to visualize the fibrous bridges that initiate the compartmentalization of liver during the progression of liver fibrosis.

3.6. Histology

Histopathological evaluation of the fibrosed liver revealed moderate to severe necrosis of hepatocytes with infiltration of mononuclear cells, perilobular fibrosis and portal triad fibrosis in liver sections (Fig. 8). Excessive collagen fibres are seen in the fibrosed area under the MT staining. Based on the H&E and MT staining procedures, the fibrous bridges dividing the liver into rounded islands of hepatic parenchyma resulting in the nodular formation surrounded by fibrous tissue has been observed in the liver. These histopathological observations reconfirm the development of fibrotic stage of liver rat model (Constandinou et al., 2005; Le Naour et al., 2012). The iron uptake by the liver macrophages which was responsible for the hypointense MR image of the liver has been confirmed by PB staining.

4. Conclusions

SPIONs stabilized with high molecular weight dextran were synthesized without compromising the particle size and magnetic properties. The developed system has an optimized core size of 12 nm and hydrodynamic size of 50 nm. These particles showed high degree of blood compatibility and less cytotoxicity on liver cells confirming its suitability to use the same as MRI contrast agent safely. Moreover, the developed particles remained stable for over a period of more than 4 months. The developed nanoparticles exhibited superparamagnetic property at room temperature and possessed r_2/r_1 ratio of 56.28. T_2 weighted MR imaging shows a signal drop of 55% in the fibrosed liver after the administration of D-SPIONs. This significantly improved the contrast difference between the fibrotic tissue and the rest of the extracellular matrix rich hepatic parenchyma at the fibrosis stage. The hyperintense streaks visualized in the hypointense fibrotic liver as a result of the contrast difference due to D-SPION uptake helps in visualizing the extent of fibrosed tissue as part of the progression of liver disease. Further studies using MRI for the quantification of liver fibrosis and detailed study on the relation of low and high molecular weight dextran imparted renal failure in animal models are in progress.

Acknowledgements

The financial support received from the BRNS, DAE, Government of India is sincerely acknowledged. Ariya Saraswathy and Shaiju S Nazeer acknowledge CSIR, New Delhi for the senior research fellowship. We also thank the Scientists in charge of BST, MIC, MOM and DTERT divisions of BMT Wing and HOD, IS &IR of SCTIMST for extending their support in using some of their facilities. The support from Dr. P. A. Joy, NCL, Pune in the VSM studies is also sincerely acknowledged.

References

Albanese, A., Tang, P. S., & Chan, W. C. W. (2012). The effect of nanoparticle size, shape, and surface chemistry on biological systems. *Annual Review of Biomedical Engineering*, *14*(14), 1–16.

Bautista, M. C., Bomati-Miguel, O., Morales, M. D., Serna, C. J., & Veintemillas-Verdaguer, S. (2005). Surface characterisation of dextran-coated iron oxide nanoparticles prepared by laser pyrolysis and coprecipitation. *Journal of Magnetism and Magnetic Materials*, *293*(1), 20–27.

Carp, O., Patron, L., Culita, D. C., Budrugeac, P., Feder, M., & Diamandescu, L. (2010). Thermal analysis of two types of dextran-coated magnetite. *Journal of Thermal Analysis and Calorimetry*, *101*(1), 181–187.

Chung, E. Y., Kim, H. M., Lee, G. H., Kwak, B. K., Jung, J. S., Kuh, H. J., et al. (2012). Design of deformable chitosan microspheres loaded with superparamagnetic iron oxide nanoparticles for embolotherapy detectable by magnetic resonance imaging. *Carbohydrate Polymers*, *90*(4), 1725–1731.

Constandinou, C., Henderson, N., & Iredale, J. P. (2005). Modeling liver fibrosis in rodents. *Methods in Molecular Medicine*, *117*, 237–250.

Curvo-Semedo, L., Brito, J. B., Seco, M. F., Costa, J. F., Marques, C. B., & Caseiro-Alves, F. (2010). The hypointense liver lesion on T2-weighted MR images and what it means. *Radiographics*, *30*(1).

Feest, T. G. (1976). Low molecular weight dextran: A continuing cause of acute renal failure. *British Medical Journal*, *2*(6047), 1300.

Gonzales, M., Mitsumori, L. M., Kushleika, J. V., Rosenfeld, M. E., & Krishnan, K. M. (2010). Cytotoxicity of iron oxide nanoparticles made from the thermal decomposition of organometallics and aqueous phase transfer with Pluronic F127. *Contrast Media & Molecular Imaging*, *5*(5), 286–293.

Gossuin, Y., Gillis, P., Hocq, A., Vuong, Q. L., & Roch, A. (2009). Magnetic resonance relaxation properties of superparamagnetic particles. *Wiley Interdisciplinary Reviews – Nanomedicine and Nanobiotechnology*, *1*(3), 299–310.

Gupta, A. K., & Wells, S. (2004). Surface-modified superparamagnetic nanoparticles for drug delivery: Preparation, characterization, and cytotoxicity studies. *IEEE Transactions on Nanobioscience*, *3*(1), 66–73.

Hradil, J., Pisarev, A., Babic, M., & Horak, D. (2007). Dextran-modified iron oxide nanoparticles. *China Particuology*, *5*(1-2), 162–168.

Jahn, M. R., Andreasen, H. B., Futterer, S., Nawroth, T., Schunemann, V., Kolb, U., et al. (2011). A comparative study of the physicochemical properties of iron isomaltoside 1000 (Monofer), a new intravenous iron preparation and its clinical implications. *European Journal of Pharmaceutics and Biopharmaceutics*, *78*(3), 480–491.

Jemal, A., Bray, F., Center, M. M., Ferlay, J., Ward, E., & Forman, D. (2011). Global cancer statistics. *CA: A Cancer Journal for Clinicians*, *61*(2), 69–90.

Kim, D. K., Mikhaylova, M., Wang, F. H., Kehr, J., Bjelke, B., Zhang, Y., et al. (2003). Starch-coated superparamagnetic nanoparticles as MR contrast agents. *Chemistry of Materials*, *15*(23), 4343–4351.

Kolios, G., Valatas, V., & Kouroumalis, E. (2006). Role of Kupffer cells in the pathogenesis of liver disease. *World Journal of Gastroenterology*, *12*(46), 7413–7420.

Le Naour, F., Sandt, C., Peng, C. Y., Trcera, N., Chiappini, F., Flank, A. M., et al. (2012). In situ chemical composition analysis of cirrhosis by combining synchrotron Fourier transform infrared and synchrotron X-ray fluorescence microspectroscopies on the same tissue section. *Analytical Chemistry*, *84*(23), 10260–10266.

Manju, S., Sharma, C. P., & Sreenivasan, K. (2011). Targeted coadministration of sparingly soluble paclitaxel and curcumin into cancer cells by surface engineered magnetic nanoparticles. *Journal of Materials Chemistry*, *21*(39), 15708–15717.

Mann, R. E., Smart, R. G., & Govoni, R. (2003). The epidemiology of alcoholic liver disease. *Alcohol Research & Health*, *27*(3), 209–219.

Marckmann, P., Skov, L., Rossen, K., Dupont, A., Damholt, M. B., Heaf, J. G., et al. (2006). Nephrogenic systemic fibrosis: Suspected causative role of gadodiamide used for contrast-enhanced magnetic resonance imaging. *Journal of the American Society of Nephrology*, *17*(9), 2359–2362.

Molday, R. S., & MacKenzie, D. (1982). Immunospecific ferromagnetic iron-dextran reagents for the labeling and magnetic separation of cells. *Journal of Immunological Methods*, *52*(3), 353–367.

Morgan, T. O., Little, J. M., & Evans, W. A. (1966). Renal failure associated with low-molecular-weight dextran infusion. *British Medical Journal*, *2*(5516), 737–739.

Nidhin, M., Nazeer, S. S., Jayasree, R. S., Kiran, M. S., Nair, B. U., & Sreeram, K. J. (2013). Flower shaped assembly of cobalt ferrite nanoparticles: Application as T2 contrast agent in MRI. *RSC Advances*, *3*(19), 6906–6912.

Piperno, A. (1998). Classification and diagnosis of iron overload. *Haematologica*, *83*(5), 447–455.

Reimer, P., & Balzer, T. (2003). Ferucarbotran (Resovist): A new clinically approved RES-specific contrast agent for contrast-enhanced MRI of the liver: Properties, clinical development, and applications. *European Radiology*, *13*(6), 1266–1276.

Reimer, P., Weissleder, R., Lee, A. S., Buettner, S., Wittenberg, J., & Brady, T. J. (1991). Asialoglycoprotein receptor function in benign liver disease: Evaluation with MR imaging. *Radiology*, *178*(3), 769–774.

Saboktakin, M. R., Tabatabaie, R., Maharramov, A., & Ramazanov, M. A. (2010). Synthesis and characterization of superparamagnetic chitosan-dextran sulfate hydrogels as nano carriers for colon-specific drug delivery. *Carbohydrate Polymers*, *81*(2), 372–376.

Saboktakin, M. R., Tabatabaie, R. M., Maharramov, A., & Ramazanov, M. A. (2010). A synthetic macromolecule as MRI detectable drug carriers: Aminodextran-coated iron oxide nanoparticles. *Carbohydrate Polymers*, *80*(3), 695–698.

Simberg, D., Park, J. H., Karmali, P. P., Zhang, W. M., Merkulov, S., McCrae, K., et al. (2009). Differential proteomics analysis of the surface heterogeneity of dextran iron oxide nanoparticles and the implications for their in vivo clearance. *Biomaterials*, *30*(23-24), 3926–3933.

Soenen, S. J. H., Hodenius, M., & De Cuyper, M. (2009). Magnetoliposomes: Versatile innovative nanocolloids for use in biotechnology and biomedicine. *Nanomedicine*, *4*(2), 177–191.

Stefanescu, R., Born, R., Moise, A., Ernst, B., & Przybylski, M. (2011). Epitope structure of the carbohydrate recognition domain of asialoglycoprotein receptor to a monoclonal antibody revealed by high-resolution proteolytic excision mass spectrometry. *Journal of the American Society for Mass Spectrometry*, *22*(1), 148–157.

Szabo, G., & Mandrekar, P. (2010). Focus on: Alcohol and the liver. *Alcohol Research & Health*, *33*(1), 87–96.

Talwalkar, J. A., Yin, M., Fidler, J. L., Sanderson, S. O., Kamath, P. S., & Ehman, R. L. (2008). Magnetic resonance imaging of hepatic fibrosis: Emerging clinical applications. *Hepatology*, *47*(1), 332–342.

Thomas, J. J., Rekha, M. R., & Sharma, C. P. (2010). Dextran-protamine polycation: An efficient nonviral and haemocompatible gene delivery system. *Colloids and Surfaces B: Biointerfaces*, *81*(1), 195–205.

Thomas, J. J., Rekha, M. R., & Sharma, C. P. (2012). Unraveling the intracellular efficacy of dextran–histidine polycation as an efficient nonviral gene delivery system. *Molecular Pharmaceutics*, *9*(1), 121–134.

Tsai, Z. T., Tsai, F. Y., Yang, W. C., Wang, J. F., Liu, C. L., Shen, C. R., et al. (2012). Preparation and characterization of ferrofluid stabilized with biocompatible chitosan and dextran sulfate hybrid biopolymer as a potential magnetic resonance imaging (MRI) T2 contrast agent. *Marine Drugs*, *10*(11), 2403–2414.

Van de Bovenkamp, M., Groothuis, G. M., Meijer, D. K., & Olinga, P. (2007). Liver fibrosis in vitro: Cell culture models and precision-cut liver slices. *Toxicology In Vitro*, *21*(4), 545–557.

Veselkin, E., Kondratyev, M., Lurie, Y., Ron, E., Santo, M., Reif, S., et al. (2011). A secreted form of the asialoglycoprotein receptor, sH2a, as a novel potential noninvasive marker for liver fibrosis. *PLoS ONE*, *6*(11).

Vu-Quang, H., Muthiah, M., Kim, Y. K., Cho, C. S., Namgung, R., Kim, W. J., et al. (2012). Carboxylic mannan-coated iron oxide nanoparticles targeted to immune cells for lymph node-specific MRI in vivo. *Carbohydrate Polymers*, *88*(2), 780–788.

Vu-Quang, H., Muthiah, M., Lee, H. J., Kim, Y. K., Rhee, J. H., Lee, J. H., et al. (2012). Immune cell-specific delivery of beta-glucan-coated iron oxide nanoparticles for diagnosing liver metastasis by MR imaging. *Carbohydrate Polymers*, *87*(2), 1159–1168.

Wan, J. Q., Jiang, X. H., Li, H., & Chen, K. Z. (2012). Facile synthesis of zinc ferrite nanoparticles as non-lanthanide T-1 MRI contrast agents. *Journal of Materials Chemistry*, *22*(27), 13500–13505.

Wang, Y. X. (2011). Superparamagnetic iron oxide based MRI contrast agents: Current status of clinical application. *Quantitative Imaging in Medicine and Surgery*, *1*(1), 35–40.

Wang, Y. X., Hussain, S. M., & Krestin, G. P. (2001). Superparamagnetic iron oxide contrast agents: Physicochemical characteristics and applications in MR imaging. *European Radiology*, *11*(11), 2319–2331.

Wang, Z., & Cuschieri, A. (2013). Tumour cell labelling by magnetic nanoparticles with determination of intracellular iron content and spatial distribution of the intracellular iron. *International Journal of Molecular Sciences*, *14*(5), 9111–9125.

Weinstein, J. S., Varallyay, C. G., Dosa, E., Gahramanov, S., Hamilton, B., Rooney, W. D., et al. (2010). Superparamagnetic iron oxide nanoparticles: Diagnostic magnetic resonance imaging and potential therapeutic applications in neurooncology and central nervous system inflammatory pathologies, a review. *Journal of Cerebral Blood Flow and Metabolism: Official Journal of the International Society of Cerebral Blood Flow and Metabolism*, *30*(1), 15–35.

Yerram, P., Saab, G., Karuparthi, P. R., Hayden, M. R., & Khanna, R. (2007). Nephrogenic systemic fibrosis: A mysterious disease in patients with renal failure-role of gadolinium-based contrast media in causation and the beneficial effect of intravenous sodium thiosulfate. *Clinical Journal of the American Society of Nephrology*, *2*(2), 258–263.

Web reference

http://www.amagpharma.com/products/feridex_iv.php, http://www.thefreelibrary.com/AMAG+Pharmaceuticals,+Inc.+Announces+Update+on+Sinerem(TM)+in+Europe.-a0172378541.